Front. Chem. Sci. Eng. 2014, 8(3): 369–377
DOI 10.1007/s11705-014-1435-9

RESEARCH ARTICLE

Highly selective catalytic hydrodeoxygenation of guaiacol to cyclohexane over Pt/TiO_2 and $NiMo/Al_2O_3$ catalysts

Zhong HE, Xianqin WANG (✉)

Department of Chemical, Biological and Pharmaceutical Engineering, New Jersey Institute of Technology, Newark, NJ 07102, USA

Abstract Catalysts Pt/TiO_2 and $NiMo/Al_2O_3$ are highly active and selective for the hydrodeoxygenation of guaiacol in a fixed bed reactor at 300 °C and 7.1 MPa, leading to the hydrogenation of aromatic ring, followed by demethylation and dehydroxylation to produce cyclohexane. For a complete hydrodeoxygenation of guaiacol, metal sites and acid sites are required. $NiMo/Al_2O_3$ and Pt/Al_2O_3 are more active and selective for cyclohexane formation as compared with Pt/TiO_2 at 285 °C and 4 MPa. However, Pt/TiO_2 is stable while the other two catalysts deactivate due to the nature and amount of coke formation during the reaction.

Keywords Pt/TiO_2, $NiMo/Al_2O_3$, Pt/Al_2O_3, bio-oil, hydrodeoxygenation, guaiacol, cyclohexane

1 Introduction

There is a growing interest in energy production from renewable resources because of energy crisis and environmental concerns [1]. Pyrolysis bio-oils have been considered as a promising second-generation biofuel to address these challenges because of the sustainability (derived from biomass) and unique properties (low content of sulphur and nitrogen). However, the high oxygen (up to 47 wt-%) content in pyrolysis oils lead to low heating value, high acidity and chemical instability [2]. Therefore, pyrolysis oils must be upgraded before being used as transportation fuels.

Guaiacol (GUA) serves as a very good model compound for bio-oil upgrading by hydrodeoxygenation (HDO) since it represents a large number of mono- and dimethoxy phenols derived from ligno-cellulosic biomass (typically ca. 30 wt-% of bio-oil is from lignin-derived phenolic components which have high energy density [3]). So far, sulfided NiMo [4–7] and CoMo [4–10] catalysts have been mostly used in GUA HDO. However, these industrial hydrotreating catalysts are not suitable for HDO of bio-oils with inherently low sulphur due to catalyst deactivation (loss of Brønsted acid and Lewis acid) and product contamination from sulphur stripping [11–13]. Thus, non-sulfided catalysts gained more attentions for GUA HDO reactions in recent years [14–18]. Among these catalysts, catalyst deactivation is a general challenge. However, transition metal oxides such as ZrO_2 suffered less coke than γ-Al_2O_3 [8,9], and Pt had less coke deposition than that on Pd and Rh over ZrO_2 [9]. Moreover, Mono-metallic Ni-based catalyst showed more than 15 wt-% carbon formation after GUA HDO [19]. Hence, a catalyst with Pt supported on transition metal oxides will be of interest to alleviate catalyst deactivation by coke for GUA HDO [20].

In our previous work, Pt supported on TiO_2 was found to have unique catalytic properties than on ZrO_2 and CeO_2 for HDO of acetic acid [21]. Pt supported on TiO_2 is employed in this work for a better understanding of GUA HDO surface chemistry, which leads to designing efficient catalysts for desired products. Reduced $NiMo/\gamma$-Al_2O_3 and Pt/Al_2O_3 are used for comparison.

2 Experimental

2.1 Catalyst preparation

Pt/TiO_2 (1 wt-%) and Pt/Al_2O_3 (1 wt-%) were prepared by incipient wetness impregnation of TiO_2 (Degussa P25) and Al_2O_3 (Degussa VP Alu 130), respectively, with a solution of $Pt(NH_3)_4(NO_3)_2$ (Strem 99%). The samples were dried at 100 °C overnight, and then calcined at 260 °C for 3 h. $NiMo/Al_2O_3$ (14 wt-% MoO_3 and 3.5 wt-% NiO) was prepared by sequential incipient wetness impregnation of Al_2O_3 with an aqueous solution of $(NH_4)_6Mo_7O_{24}\cdot 4H_2O$, followed by an aqueous solution of $Ni(NO_3)_2\cdot 6H_2O$. The

Received April 5, 2014; accepted April 10, 2014

E-mail: xianqin@njit.edu

catalyst was dried in air at ambient temperature for 4 h, then dried at 120 °C for 12 h, and finally was calcined at 500 °C for 4 h. The commercial $CoMo/Al_2O_3$ (4.4 wt-% CoO, 11.9 wt-% MoO_3) was from Strem Chemicals.

2.2 Characterization

X-ray diffraction (XRD) was collected using a Philips PW3040 X-ray diffractometer with Cu Kα radiation (λ = 1.54 Å) operated at 45 kV and 40 mA. The data was scanned in the range of 2θ = 10°–90°. NH_3/H_2 temperature-programmed desorption (TPD) and Temperature-programmed reduction (TPR) were performed to the reduced samples (fresh samples for TPR) by an AutoChem 2920 II with an on-line mass spectrometer (QMS 200, Stanford Research Systems). Temperature-programmed oxidation (TPO) was carried out after the reaction is finished. The catalyst was heated to 700 °C at a rate of 7 °C/min in a 10 vol-% O_2/He stream at 50 sccm, and the signal of m/z 44 (CO_2) was monitored and recorded using an on-line mass spectrometer.

2.3 Catalyst testing

Pt/TiO_2, $CoMo/Al_2O_3$ and $NiMo/Al_2O_3$ were reduced at 350, 420, and 380 °C, respectively, for one hour before the activity test in a fixed-bed reactor with inner diameter of 9.4 mm. 100 sccm of H_2 was used as the carrier gas, a liquid feed of GUA was premixed with dodecane and was introduced to the reaction system by a liquid pump at the rate of 5.4 mL/h. 0.2 g catalysts were loaded for the reactions at 300 °C and 7.1 MPa (3 wt-% GUA), while 0.1 g samples were used for the reactions at 285 °C and 4 MPa (10 wt-% GUA). The liquid products were drained every one hour for analysis by an Agilent GC 7890A, while the gas products were analyzed automatically during the reaction. The 1 microliter of liquid samples was injected to GC with a split mode of ratio of 1:100. The oven temperature was heated from 50 °C to 90 °C with a ramp of 10 °C/min, then to 250 °C with a ramp of 60 °C/min, and held at 250 °C for 1 min. The GC was equipped with an FID with a HP-5 column, and a TCD with a HP-PLOT/Q column.

2.4 Data analysis

The conversion of GUA was calculated based on Eq. (1). The product selectivity (S, mol-%)) was calculated by the Eq. (2), where the unreacted GUA was not included. The degree of HDO (%) was calculated with Eq. (3). The selectivity of cyclohexane was calculated by Eq. (4).

$$X_{\mathrm{GUA}} = \frac{(N_{\mathrm{GUA}})_{\mathrm{in}} - (N_{\mathrm{GUA}})_{\mathrm{out}}}{(N_{\mathrm{GUA}})_{\mathrm{in}}} \times 100, \quad (1)$$

$$S_i(\%) = \frac{\text{moles of carbon in product } i}{\text{the sum of caron moles in products}} \times 100, \quad (2)$$

$$\mathrm{HDO} = \frac{2 \times (N_{\mathrm{GUA}})_{\mathrm{in}} - \sum_{i=j}^{m} N_{(i)\mathrm{produced}} b_i}{2 \times (N_{\mathrm{GUA}})_{\mathrm{in}}} \times 100, \quad (3)$$

$$S_{\mathrm{cyclohexane}} = \frac{6 \times \left(N_{\mathrm{cyclohexane}}\right)_{\mathrm{out}}}{7 \times (N_{\mathrm{GUA}})_{\mathrm{converted}}} \times 100, \quad (4)$$

where $(N_{\mathrm{GUA}})_{\mathrm{in}}$ is the initial amount of GUA (mol), $(N_{\mathrm{GUA}})_{\mathrm{out}}$ was the final amount of GUA (mol), b_i was the number of oxygen atoms in the molecule of ith product, and $\sum_{i=j}^{m} N_{(i)\mathrm{produced}}$ = total moles of main products including cyclohexane, methane, cyclohexanol, methyl-cyclopentane, methyl-cyclohexane. Unreacted GUA was included in calculation of HDO degree.

O/C and H/C molar ratios after GUA HDO reaction were calculated by Eqs. (5) and (6) for the main liquid phase. Methane is not included in the calculation.

$$\mathrm{O/C(mol/mol)} = \frac{\sum n(\text{oxygen})\text{unreacted GUA and main products}}{\sum n(\text{carbon})\text{unreacted GUA and main products}}, \quad (5)$$

$$\mathrm{H/C(mol/mol)} = \frac{\sum n(\text{hydrogen})\text{unreacted GUA and main products}}{\sum n(\text{carbon})\text{unreacted GUA and main products}}. \quad (6)$$

3 Results and discussion

3.1 Characterization

3.1.1 H_2-TPD

H_2-TPD is used to study the types (chemisorbed hydrogen on metal sites, or spillover hydrogen present on the supports) and quantities of hydrogen on the supported metal catalysts as shown in Fig. 1(a). The hydrogen peak over Pt/TiO_2 catalyst at 300 °C corresponds to the H_2 adsorbed on Pt particles while the one at 450 °C is assigned to hydrogen spilled over from Pt to TiO_2 since the support is irreversibly dehydroxylated at high temperatures. H_2 desorption peaks at 460–480 °C over $NiMo/Al_2O_3$ and $CoMo/Al_2O_3$ are assigned to spillover hydrogen from Ni or Co. According to the literature [22], the quantity of spillover hydrogen depends on the number of hydroxyl groups on the support and is larger on acidic supports. The hydrogen desorption amount is in agreement with NH_3-TPD for $NiMo/Al_2O_3$ and $CoMo/Al_2O_3$ catalysts in Fig. 1

(b). However, The H_2 desorption from supports by H_2-TPD is not consistent with the amount of acid sites by NH_3-TPD in quantity since NH_3-TPD shows a total amount of acid sites instead of Brønsed acid sites. H_2 desorption from Ni and Co is at 300 °C and 370 °C, respectively. Based on the H_2 desorption amount and temperature, the ability for hydrogen dissociation at ~300 °C followed the sequence: $Pt/TiO_2 > NiMo/Al_2O_3 > CoMo/Al_2O_3$.

3.1.2 NH_3-TPD

NH_3-TPD profiles of $CoMo/Al_2O_3$, $NiMo/Al_2O_3$, Pt/TiO_2 and Pt/Al_2O_3 are shown in Fig. 1(b). Only two NH_3 desorption peaks are observed on Pt/TiO_2, one at ~300 °C and another at ~570 °C, which could be assigned to moderate and strong acid sites, respectively. Both $CoMo/Al_2O_3$ and $NiMo/Al_2O_3$ have three NH_3 desorption peaks. The first one corresponds to NH_3 adsorbed on moderate acid sites, while the other two are assigned to strong acid sites. The strength of these three acids is very similar on $NiMo/Al_2O_3$ and $CoMo/Al_2O_3$. Furthermore, $NiMo/Al_2O_3$ has more acid sites as compared with that of $CoMo/Al_2O_3$ due to the different sources of Al_2O_3 ($CoMo/Al_2O_3$ is a commercial catalyst from Strem Chemicals, while $NiMo/Al_2O_3$ is homemade with the Al_2O_3 from Degussa). Pt/Al_2O_3 has mainly weak and moderate acid sites, but the amount of the acid sites is much more than that on the other two Al_2O_3-based catalysts. In addition, more strong acid sites are present on Pt/Al_2O_3 than that on Pt/TiO_2 (with a desorption temperature centered at 550 °C).

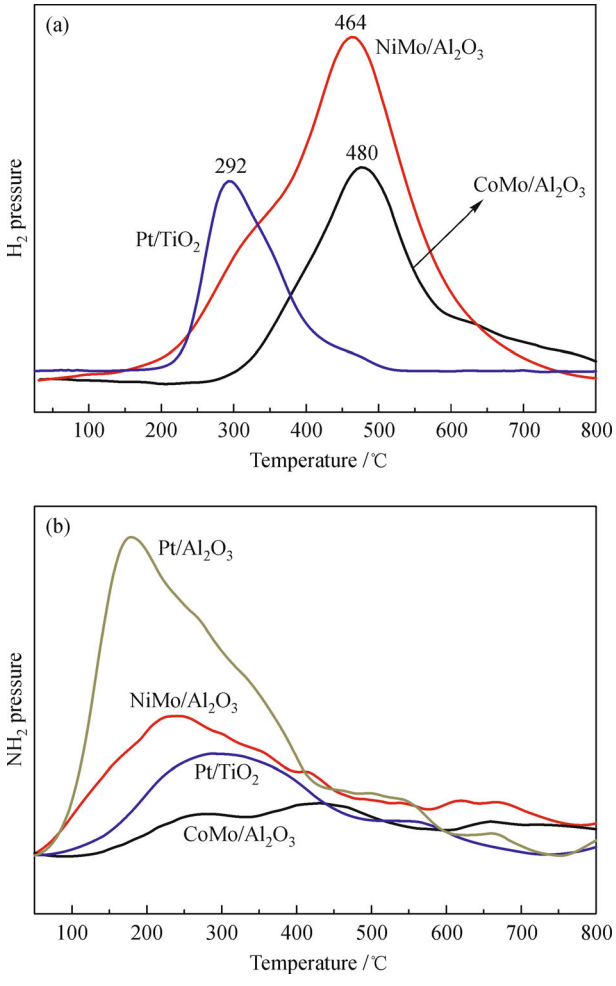

Fig. 1 (a) H_2-TPD profiles of the $CoMo/Al_2O_3$, $NiMo/Al_2O_3$ and Pt/TiO_2 catalysts, (b) NH_3-TPD profiles of $CoMo/Al_2O_3$, $NiMo/Al_2O_3$ and Pt/TiO_2

3.1.3 H_2-TPR

The H_2 and H_2O concentration profiles are presented in Fig. 2. Three water peaks at 160 °C, 460 °C, 800 °C and two H_2 consumption peaks at 380 °C and 750 °C could be observed over the $NiMo/Al_2O_3$ catalyst. The peak at 160 °C is from the water on the catalyst, while the water peak at 460 °C with the H_2 consumption peak at 380 °C is assigned to the reduction of NiO species, the last water peak and H_2 consumption peak corresponds to MoO_3 reduction. $CoMo/Al_2O_3$ shows similar reduction behaviors to that for the $NiMo/Al_2O_3$ catalyst. However, CoO is reduced at a higher temperature (400 °C).

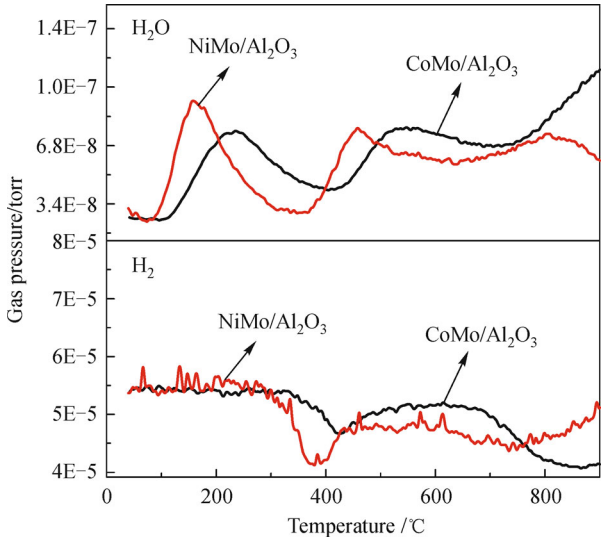

Fig. 2 TPR profiles of the $CoMo/Al_2O_3$ and $NiMo/Al_2O_3$ catalysts

3.1.4 XRD

Figure 3 presents the XRD patterns of raw Pt/TiO_2, reduced Pt/TiO_2 and used Pt/TiO_2 after reaction. Two main TiO_2 phases — anatase (with a mark of A) and rutile (with a mark of R) were observed in Pt/TiO_2 catalysts. The main phases of TiO_2 are not changed obviously after reduction.

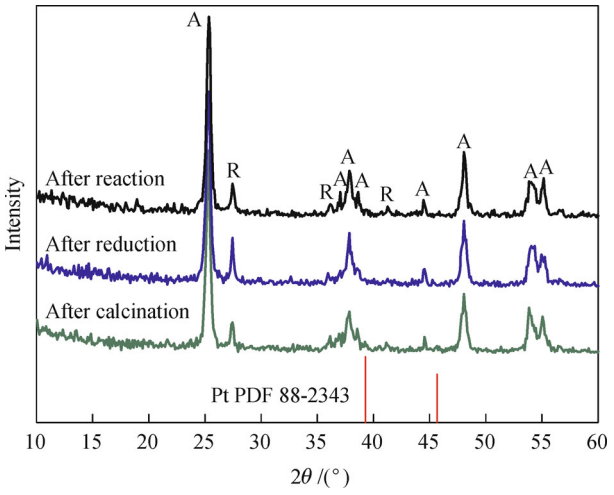

Fig. 3 X-ray Diffraction pattern of the Pt/TiO_2 catalysts

Pt characteristic peaks are detected at 39.2° and 45.7° after calcination, suggesting that PtO_x underwent auto-reduction during calcination. However, these two diffraction peaks disappear after reduction and even after reaction, indicating that reduction with H_2 promotes the dispersion of Pt particles and their average size does not increase even after reaction.

Three prominent peaks which appeared at 2θ = 37.6°, 45.8° and 66.8° (PDF 29-1486) for three samples are from γ-Al_2O_3 (Fig. 4). For the freshly prepared $NiMo/Al_2O_3$, the diffraction peak at 2θ of 39.4° is assigned to γ-Al_2O_3, The diffraction peak at 43.4° indicates the presence of NiO in the $NiMo/Al_2O_3$ catalyst after calcination and after reaction. However, this peak is much weaker after reduction, indicating that Ni species are partially metallic in $NiMo/Al_2O_3$ after reduction. This observation is also confirmed by the sharper peak at 45.5° in the reduced sample which corresponds to metallic Ni. MoO_3 diffraction peaks between 32.5°–35° are not detected in all

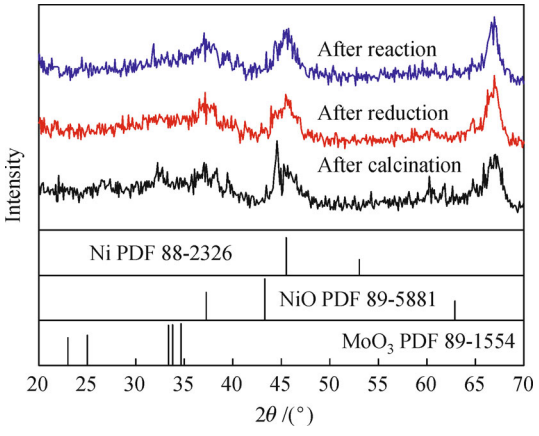

Fig. 4 X-ray Diffraction pattern of the $NiMo/Al_2O_3$ catalysts

samples, indicating that MoO_3 is highly dispersed in the $NiMo/Al_2O_3$ catalyst. The structure of Al_2O_3 does not change obviously regardless of the reaction or the reduction, suggesting Al_2O_3 is very stable.

3.2 Reactivity

Pt/TiO_2 and $NiMo/Al_2O_3$ were tested at 300 °C, 7.1 MPa for five hours to investigate the catalyst activity and stability. GUA HDO over commercial $CoMo/Al_2O_3$ and a blank run without catalysts are used as a reference. The blank run with dodecane solvent under our reaction conditions showed negligible contribution.

The conversions of the GUA obtained from three catalysts and blank run are shown in Fig. 5(a). All catalysts require three hours to reach a stable GUA conversion. Catalysts improve the conversion of GUA dramatically compared with that from blank run. The conversions of GUA on Pt/TiO_2 and $NiMo/Al_2O_3$ are similar and very high (96%). A stable conversion of 73% is obtained over commercial $CoMo/Al_2O_3$. The reason why the reduced $NiMo/Al_2O_3$ has higher activity than $CoMo/Al_2O_3$ is mainly due to more hydrogenation active sites on $NiMo/Al_2O_3$ as it has more CO adsorption compared with that on $CoMo/Al_2O_3$ in CO pulse chemisorption. High activity of Pt/TiO_2 could be explained by particular efficiency in activation of molecular hydrogen by Pt (Fig. 1(a)) and the C–O single bond activation by phase boundary type active sites on the boundary between Pt and TiO_2 [21].

H/C and O/C molar ratios of GUA products and HDO degree for liquid products are listed in Table 1. The GUA HDO degrees are 88% and 94% over Pt/TiO_2 and $NiMo/Al_2O_3$, respectively. However, the blank run showed only 7% HDO degree. The H/C and O/C molar ratios in the liquid product over $NiMo/Al_2O_3$ and Pt/TiO_2 catalysts are similar to those of gasoline and diesel. This observation implies both $NiMo/Al_2O_3$ and Pt/TiO_2 have very good GUA conversion and high selectivity for oxygen elimination in HDO reactions.

3.3 Product distributions

The distributions of main products on Pt/TiO_2 and $NiMo/Al_2O_3$ as a function of time on stream (TOS) are presented in Figs. 5(b) and 5(c), respectively. Similar trends in GUA transformation and product distribution are observed over Pt/TiO_2 and $NiMo/Al_2O_3$. The selectivity of cyclohexane decreases while methane increases as a function of TOS. The decrease of cyclohexane amount is mainly due to the coke deposits [1)] while methane could be still produced from these deposits with the presence of hydrogen at a high pressure and temperature. Methyl-cyclopentane, methyl-cyclohexane and cyclohexanol stay nearly constant during

1) He Z, Wang X. Highly effective hydrodeoxygenation of guaiacol on Pt/TiO_2: Promoter effects. In preparation

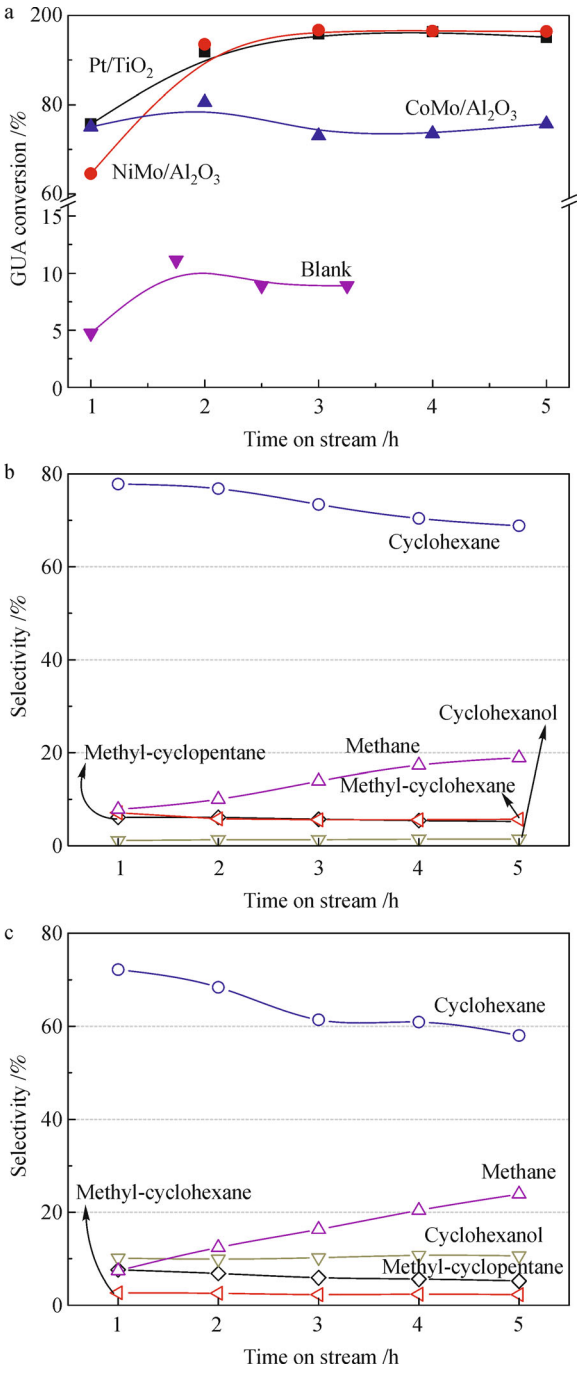

Fig. 5 (a) GUA conversion versus time on steam, (b) Product distribution of the main products from GUA HDO over $NiMo/Al_2O_3$, (c) Product distribution of the main products from GUA HDO over Pt/TiO_2.

the test. $NiMo/Al_2O_3$ has a higher selectivity to cyclohexane and methyl-cyclohexane while a lower selectivity to methane and cyclohexanol, as compared with those from Pt/TiO_2. It is noteworthy that cyclohexanol concentration is much higher from Pt/TiO_2 (close to 11%) than that from $NiMo/Al_2O_3$ (1.4%), leading to a higher O/C molar ratio of the product mixture. Thus, the conversion of cyclohexanol

Table 1 H/C and O/C molar ratios of GUA products and HDO degree

Samples	H/C	O/C	HDO degree /%
Blank run[a]	1.27	0.25	7.4
Pt/TiO_2[a]	2.02	0.04	88.1
$NiMo/Al_2O_3$[a]	2.03	0.02	94.3
Liquid feed (3 wt-%)	1.14	0.29	–
Gasoline	1~2	~ 0	–
Diesel	~2	~0	–

[a] Data are collected when HDO occurred for three hours. Reaction conditions: H_2 pressure, 7.1 MPa; temperature, 300 °C.

to cyclohexane is more favorable over $NiMo/Al_2O_3$ than over Pt/TiO_2, which is consistent with [3], more acidity favors dehydration of cyclohexanol to cyclohexene, suggesting clyclohexanol dehydration might be a rate limiting step during GUA HDO. $NiMo/Al_2O_3$ has more acid sites than Pt/TiO_2 (Fig. 1(b)). Thus, $NiMo/Al_2O_3$ has a higher cyclohexane concentration and a lower cyclohexanol concentration (Fig. 5).

3.4 Reaction pathway and mechanism

Based on the literature [3,7,23] and the products from GUA HDO experiments, a reaction network for GUA HDO over the Pt/TiO_2 and $NiMo/Al_2O_3$ catalysts is proposed (Fig. 6). The compounds that are not detected in the liquid products during the reaction are presented in brackets. However, these compounds are likely to be the intermediates responsible for the formation of the identified final products. On sulfided CoMo and NiMo catalysts, GUA HDO started with demethylation or demethoxylation and deoxygenation, followed by the benzene ring hydrogenation [7,11,24,25]. However, hydrogenation of the GUA's benzene ring was reported to be the first step over Rh-based catalysts [7,23] and Pd-based catalysts [26], followed by demethoxylation, demethylation or dehydroxylation. Benzene ring hydrogenation in the phenol HDO was seen over Pt supported catalysts [27,28]. Here, hydrogenation of the GUA's benzene ring to methoxycyclohexanol may be the first step of GUA HDO over the Pt/TiO_2 and $NiMo/Al_2O_3$ catalysts since no liquid products with the benzene ring are identified. However, demethylation and dehydroxylation from methoxycyclohexanol occur in parallel, and demethoxylation may not take place due to no methanol formation, leading to two major pathways to produce cyclohexane: (1) Instead of forming cyclohexanol as an intermediate by demethoxylation, 1,2-cyclohexanediol could be the intermediate from 2-methoxycyclohexanol to cyclohexanol by demethylation, producing methane as the gas product (Fig. 3). Cyclohexane could be further produced from cyclohexanol by dehydration and then hydrogenation [3,29,30]. (2) The methyl group transfers from methoxy group to the cyclohexane ring on acid sites

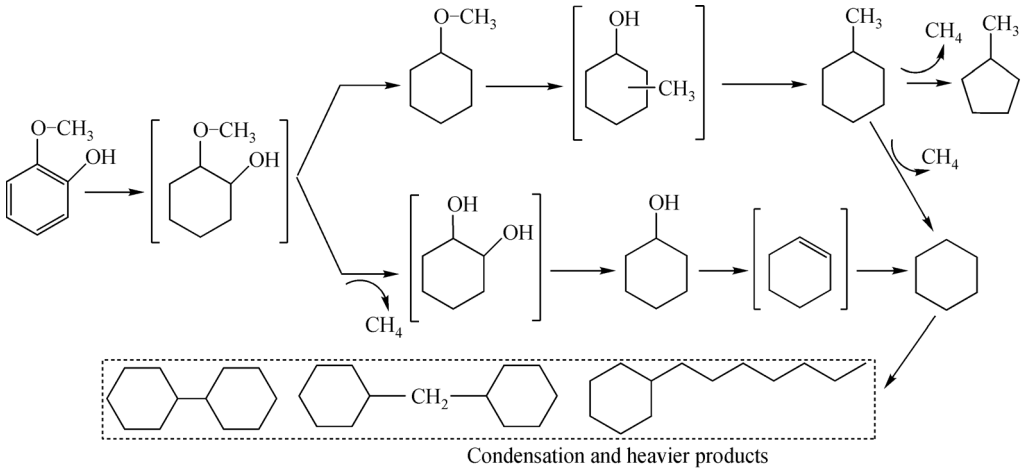

Fig. 6 Reaction network for cyclohexane formation over Pt/TiO_2

[31], followed by deoxygenation to methylcyclohexane, and undergoes further demethylation to cyclohexane, or to methylcyclopentane. Some of the cyclohexane undergoes condensation to form heavier products [27,32].

A schematic of the reaction steps is proposed for GUA HDO to cyclohexane over the Pt/TiO_2 catalyst (Fig. 7). GUA is adsorbed on Pt-TiO_2 interface by the oxygen from –OH group, which agrees with the literature [33] that the oxygen in the hydroxide group is more active than the one in the methoxy group in the GUA molecule, and causes a

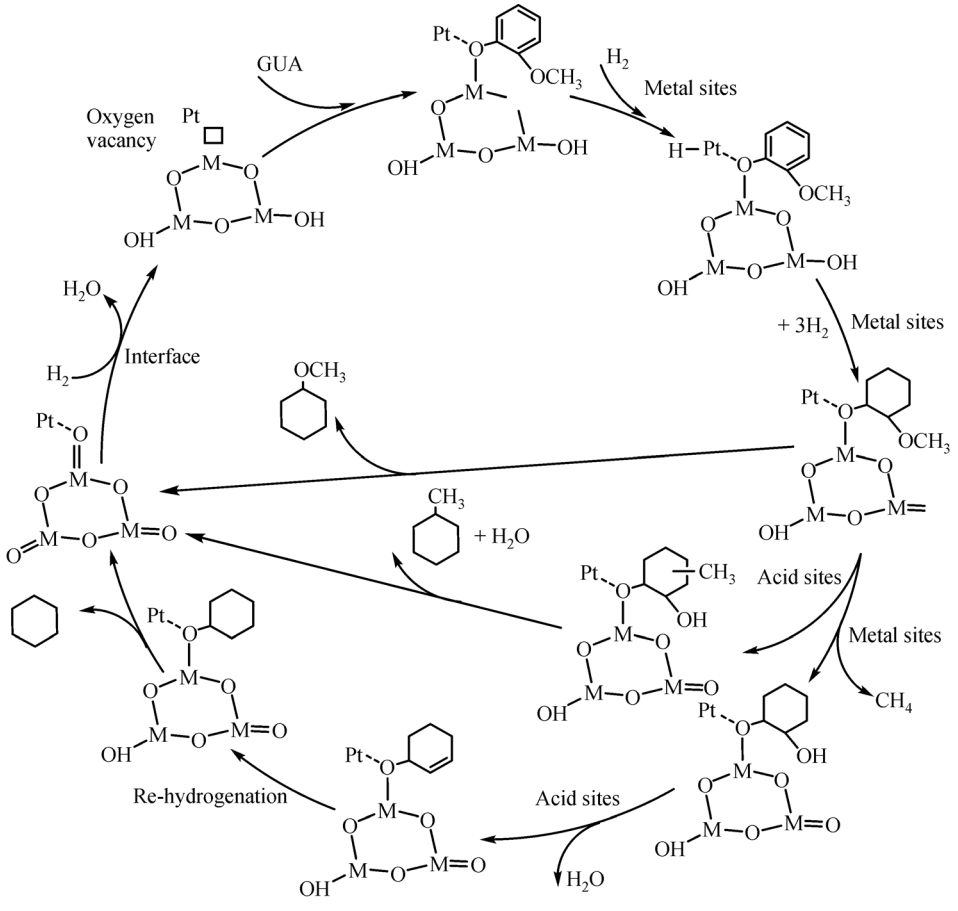

Fig. 7 Schematic representation of mechanism of the selective HDO of GUA to cyclohexane over Pt/TiO_2 catalyst

stable adsorption through the OH group on metal oxides, such as SiO_2, Al_2O_3 or SiO_2-Al_2O_3. However, Oxygen vacancies are present on reducible oxides, and oxygen in the oxy-compounds is more easily to be filled in the vacancies, such as acetic acid over Pt/TiO_2 [34] and acrolein over metal oxide bronzes [35]. These studies indicate that the adsorption of oxygen via filling the oxygen vacancies is easier and more stable than the direct oxygen adsorption to metal atoms from the supports when the catalysts contain oxygen vacancies. The adsorption sites of –OH group are proposed at the oxygen vacancy sites on TiO_2, while Pt dissociates H_2 to H that spills over to the interface, where the catalytic reactions occur. The acid promotes the dehydration of cyclohexanol species, and allows for further hydrogenation to produce cyclohexane. Our previous results [36] indicate that the interaction between Pt and TiO_2 is weak, and Pt species can be reduced at a temperature below 170 °C. Thus, Pt is proposed as in metallic state during the reactions (285–300 °C with pure hydrogen at a pressure of 4.0 MPa–7.1 MPa). As noble metal supported on Al_2O_3 has nearly no oxygen vacancy [37], non-precious metals NiMo supported on Al_2O_3 probably has no oxygen vacancies as well. Thus, the reaction steps in Fig. 7 are not applicable to $NiMo/Al_2O_3$. However, GUA adsorption on $NiMo/Al_2O_3$ is probably through the oxygen adsorption from hydroxyl group on Lewis acid sites [38], followed by dissociated H_2 by Ni. MoO_3 weakens the interaction between Ni and Al_2O_3, thus promotes the reduction of NiO and thus hydrogenation during the reactions [39]. The function of Ni for hydrogen dissociation and acid sites for dehydration are involved in cyclohexane formation, which is similar to those in Fig. 7 since the product distributions are very similar to those from Pt/TiO_2.

3.5 Performance of Pt/TiO_2 and $NiMo/Al_2O_3$

The GUA conversions over Pt/TiO_2, $NiMo/Al_2O_3$ catalyst at 300 °C and 7.1 MPa are almost 100%. To avoid extra catalyst active sites during the reactions and achieve a better comparison for GUA HDO performance, the GUA concentration in feed is increased from 3% to 10%, and the operation conditions are changed to 285 °C and 4 MPa. The tests are carried out over Pt/TiO_2, $NiMo/Al_2O_3$ and Pt/Al_2O_3 (Fig. 8(a)). Here, Pt/Al_2O_3 is used as reference for further confirmation of the acidity effect on the reactions. $NiMo/Al_2O_3$ is more active than Pt/TiO_2 at 285 °C. However, $NiMo/Al_2O_3$ starts to deactivate after three hours. Cyclohexane selectivity follows the same trend as the activity in Fig. 8(b). The activity decreases on $NiMo/Al_2O_3$ is due to the active and graphitic coke that desorbs at temperature between 400 °C and 600 °C range, and above 600 °C, respectively during TPO experiments. Pt/Al_2O_3 has a higher activity than Pt/TiO_2 but deactivates continuously along the reaction. The larger amount of coke formation on Pt/Al_2O_3 would be the main reason

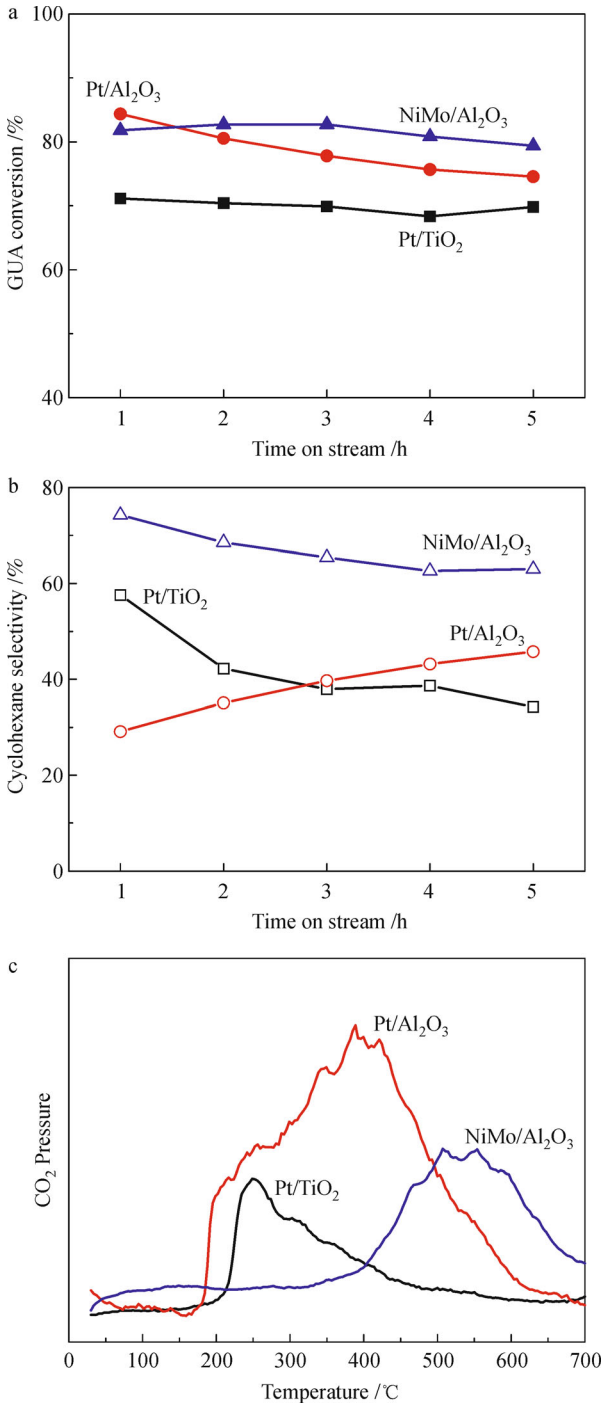

Fig. 8 (a) GUA conversion versus TOS over Pt/Al_2O_3, Pt/TiO_2 and $NiMo/Al_2O_3$, (b) Cyclohexane selectivity versus TOS over Pt/Al_2O_3, Pt/TiO_2 and $NiMo/Al_2O_3$, (c) TPO profile after reactions over Pt/Al_2O_3, Pt/TiO_2 and $NiMo/Al_2O_3$.

(Fig. 8(c)) for deactivation (Others such as sintering are possible but could be minor). This agrees with the literature that Al_2O_3 is apt to more coke formation in GUA HDO than transition metal oxides [9,40] or silica [41]. However, a high amount of acid sites (Fig. 1) in Al_2O_3 favors dehydration of cyclohexanol to form

cyclohexene, which is further hydrogenated to cyclohexane. Thus, an increase of cyclohexane selectivity is observed in Fig. 8(b). Pt/TiO_2 has lower activity and selectivity than the Al_2O_3 based catalysts. However, it is stable during the reaction because there is less coke formation and the carbon species are active carbon which desorbs at temperatures below 400 °C during TPO experiments. In short, the active coke at 300 °C over Pt/TiO_2 is mainly thermal carbon species, while the coke over $NiMo/Al_2O_3$ is primarily catalytic coke including graphitic carbon, and the coke over Pt/Al_2O_3 contains both of types [42–44].

Overall, Al_2O_3, without surface acidity modification, is not a suitable support for GUA HDO reaction since strong acidity on the surface causes a large amount of coke formation. However, following the Sabatier rule, a modified Al_2O_3, or a mixed oxide system with a medium strength of acidity can be a good support for the HDO system. The fact that $NiMo/Al_2O_3$ has a better performance than Pt/Al_2O_3 (higher activity and selectivity with less coke formation) confirms the observation, also indicating that bimetallic catalysts on TiO_2 might be more promising than mono-metallic catalysts in HDO reactions.

4 Conclusions

Pt/TiO_2 and $NiMo/Al_2O_3$ are highly active and selective for cyclohexane formation during GUA HDO at 300 °C and 7.1 MPa. The reactions go through aromatic ring hydrogenation first, followed by demethylation and dehydroxylation to produce cyclohexane. The liquid products have the similar O/C and H/C molar ratios of those for gasoline and diesel. GUA HDO requires some conditions for complete HDO: metal sites such as Ni or Pt to dissociate hydrogen, acid sites from the supports for dehydration of cyclohexanol to cyclohexene. $NiMo/Al_2O_3$ and Pt/Al_2O_3 are more active and selective for cyclohexane formation compared with Pt/TiO_2 at 285 °C and 4 MPa. However, Pt/TiO_2 is stable while the other two deactivate due to the nature and amount of coke formation during the reaction.

Acknowledgements This work was financially supported by Dr. Wang's NJIT startup package. The authors thank Yong Pu for GC-MS analysis to clarify the product species, and Jinwen Liu, Zafar Iqbal, George Barnes and Yogesh Gandhi at NJIT for their help during experiments.

References

1. Kunkes E L, Simonetti D A, West R M, Serrano-Ruiz J C, Gärtner C A, Dumesic J A. Catalytic conversion of biomass to monofunctional hydrocarbons and targeted liquid-fuel classes. Science, 2008, 322 (5900): 417–421
2. Furimsky E. Catalytic hydrodeoxygenation. Applied Catalysis A, General, 2000, 199(2): 147–190
3. Zhao C, He J, Lemonidou A A, Li X, Lercher J A. Aqueous-phase hydrodeoxygenation of bio-derived phenols to cycloalkanes. Journal of Catalysis, 2011, 280(1): 8–16
4. Laurent E, Delmon B. Study of the hydrodeoxygenation of carbonyl, carboxylic and guaiacyl groups over sulfided CoMo/γ-Al_2O_3 and NiMo/γ-Al_2O_3 catalyst. II. Influence of water, ammonia and hydrogen sulfide. Applied Catalysis A, General, 1994, 109(1): 97–115
5. Laurent E, Delmon B. Study of the hydrodeoxygenation of carbonyl, carboxylic and guaiacyl groups over sulfided CoMo/γ-Al_2O_3 and NiMo/γ-Al_2O_3 catalysts. I. Catalytic reaction schemes. Applied Catalysis A, General, 1994, 109(1): 77–96
6. Bui V N, Laurenti D, Delichère P, Geantet C. Hydrodeoxygenation of guaiacol. Applied Catalysis B: Environmental, 2011, 101(3–4): 246–255
7. Lin Y C, Li C L, Wan H P, Lee H T, Liu C F. Catalytic hydrodeoxygenation of guaiacol on Rh-based and sulfided CoMo and NiMo catalysts. Energy & Fuels, 2011, 25(3): 890–896
8. Centeno A, Laurent E, Delmon B. Influence of the support of CoMo sulfide catalysts and of the addition of potassium and platinum on the catalytic performances for the hydrodeoxygenation of carbonyl, carboxyl, and guaiacol-type molecules. Journal of Catalysis, 1995, 154(2): 288–298
9. Gutierrez A, Kaila R K, Honkela M L, Slioor R, Krause A O I. Hydrodeoxygenation of guaiacol on noble metal catalysts. Catalysis Today, 2009, 147(3–4): 239–246
10. Jongerius A L, Jastrzebski R, Bruijnincx P C A, Weckhuysen B M. CoMo sulfide-catalyzed hydrodeoxygenation of lignin model compounds: An extended reaction network for the conversion of monomeric and dimeric substrates. Journal of Catalysis, 2012, 285 (1): 315–323
11. Şenol O İ, Ryymin E M, Viljava T R, Krause A O I. Effect of hydrogen sulphide on the hydrodeoxygenation of aromatic and aliphatic oxygenates on sulphided catalysts. Journal of Molecular Catalysis A Chemical, 2007, 277(1–2): 107–112
12. Şenol O İ, Viljava T R, Krause A O I. Effect of sulphiding agents on the hydrodeoxygenation of aliphatic esters on sulphided catalysts. Applied Catalysis A, General, 2007, 326(2): 236–244
13. Bridgwater A V. Catalysis in thermal biomass conversion. Applied Catalysis A, General, 1994, 116(1–2): 5–47
14. Zhao H Y, Li D, Bui P, Oyama S T. Hydrodeoxygenation of guaiacol as model compound for pyrolysis oil on transition metal phosphide hydroprocessing catalysts. Applied Catalysis A, General, 2011, 391(1–2): 305–310
15. González-Borja M A, Resasco D E. Anisole and guaiacol hydrodeoxygenation over monolithic Pt-Sn catalysts. Energy & Fuels, 2011, 25(9): 4155–4162
16. Filley J, Roth C. Vanadium catalyzed guaiacol deoxygenation. Journal of Molecular Catalysis A Chemical, 1999, 139(2–3): 245–252
17. Bykova M V, Bulavchenko O A, Ermakov D Y, Lebedev M Y, Yakovlev V A, Parmon V N. Guaiacol hydrodeoxygenation in the presence of Ni-containing catalysts. Catalysis in Industry, 2011, 3 (1): 15–22
18. Ghampson I T, Sepúlveda C, Garcia R, Frederick B G, Wheeler M

C, Escalona N, DeSisto W J. Guaiacol transformation over unsupported molybdenum-based nitride catalysts. Applied Catalysis A, General, 2012, 413–414(31): 78–84
19. Bykova M V, Ermakov D Y, Kaichev V V, Bulavchenko O A, Saraev A A, Lebedev M Y, Yakovlev V A. Ni-based sol-gel catalysts as promising systems for crude bio-oil upgrading: Guaiacol hydrodeoxygenation study. Applied Catalysis B: Environmental, 2012, 113–114: 296–307
20. He Z, Wang X. Hydrodeoxygenation of model compounds and catalytic systems for pyrolysis bio-oils upgrading. Catalysis for Sustainable Energy, 2012, 1: 28–52
21. He Z, Wang X. Required catalytic properties for alkane production from carboxylic acids: Hydrodeoxygenation of acetic acid. Journal of Energy Chemistry, 2013, 22(6): 883–894
22. Miller J T, Meyers B L, Modica F S, Lane G S, Vaarkamp M, Koningsberger D C. Hydrogen temperature-programmed desorption (H_2 TPD) of supported platinum catalysts. Journal of Catalysis, 1993, 143(2): 395–408
23. Lee C R, Yoon J S, Suh Y W, Choi J W, Ha J M, Suh D J, Park Y K. Catalytic roles of metals and supports on hydrodeoxygenation of lignin monomer guaiacol. Catalysis Communications, 2012, 17: 54–58
24. Viljava T R, Saari E R M, Krause A O I. Simultaneous hydrodesulfurization and hydrodeoxygenation: Interactions between mercapto and methoxy groups present in the same or in separate molecules. Applied Catalysis A, General, 2001, 209(1–2): 33–43
25. Viljava T R, Komulainen R S, Krause A O I. Effect of H_2S on the stability of $CoMo/Al_2O_3$ catalysts during hydrodeoxygenation. Catalysis Today, 2000, 60(1–2): 83–92
26. Hong Y K, Lee D W, Eom H J, Lee K Y. The catalytic activity of $Pd/WOx/\gamma\text{-}Al_2O_3$ for hydrodeoxygenation of guaiacol. Applied Catalysis B: Environmental, 2014, 150–151: 438–445
27. Hong D Y, Miller S J, Agrawal P K, Jones C W. Hydrodeoxygenation and coupling of aqueous phenolics over bifunctional zeolite-supported metal catalysts. Chemical Communications, 2010, 46(7): 1038–1040
28. Sepúlveda C, Leiva K, García R, Radovic L R, Ghampson I T, DeSisto W J, Fierro J L G, Escalona N. Hydrodeoxygenation of 2-methoxyphenol over Mo_2N catalysts supported on activated carbons. Catalysis Today, 2011, 172(1): 232–239
29. Zhao C, Kou Y, Lemonidou A A, Li X, Lercher J A. Highly selective catalytic conversion of phenolic bio-oil to alkanes. Angewandte Chemie, 2009, 121(22): 4047–4050
30. Shin E J, Keane M A. Gas-phase hydrogenation/hydrogenolysis of phenol over supported nickel catalysts. Industrial & Engineering Chemistry Research, 2000, 39(4): 883–892
31. Zhu X, Lobban L L, Mallinson R G, Resasco D E. Bifunctional transalkylation and hydrodeoxygenation of anisole over a Pt/HBeta catalyst. Journal of Catalysis, 2011, 281(1): 21–29
32. Zhao C, Lercher J A. Upgrading pyrolysis oil over Ni/HZSM-5 by cascade reactions. Angewandte Chemie International Edition, 2012, 51(24): 5935–5940
33. Popov A, Kondratieva E, Goupil J M, Mariey L, Bazin P, Gilson J P, Travert A, Maugé F. Bio-oils hydrodeoxygenation: Adsorption of phenolic molecules on oxidic catalyst supports. Journal of Physical Chemistry C, 2010, 114(37): 15661–15670
34. Pestman R, Koster R M, Pieterse J A Z, Ponec V. Reactions of carboxylic acids on oxides: 1. Selective hydrogenation of acetic acid to acetaldehyde. Journal of Catalysis, 1997, 168(2): 255–264
35. Thibodeau T J, Canney A S, DeSisto W J, Wheeler M C, Amar F G, Frederick B G. Composition of tungsten oxide bronzes active for hydrodeoxygenation. Applied Catalysis A, General, 2010, 388(1–2): 86–95
36. He Z, Yang M, Wang X, Zhao Z, Duan A. Effect of the transition metal oxide supports on hydrogen production from bio-ethanol reforming. Catalysis Today, 2012, 194(1): 2–8
37. Mattos L V, Rodino E, Resasco D E, Passos F B, Noronha F B. Partial oxidation and CO_2 reforming of methane on Pt/Al_2O_3, Pt/ZrO_2, and $Pt/Ce\text{-}ZrO_2$ catalysts. Fuel Processing Technology, 2003, 83(1–3): 147–161
38. Mortensen P M, Grunwaldt J D, Jensen P A, Knudsen K G, Jensen A D. A review of catalytic upgrading of bio-oil to engine fuels. Applied Catalysis A, General, 2011, 407(1–2): 1–19
39. Yang J, Chen M, Ren J. Effect of Mo, W addition on performance of Ni/Al_2O_3 catalyst for hydrodeoxygenation. Chemical Industry and Engineering Progress, 2005, 24(12): 1386–1389
40. Bui V N, Laurenti D, Delichère P, Geantet C. Hydrodeoxygenation of guaiacol. Part II: Support effect for CoMoS catalysts on HDO activity and selectivity. Applied Catalysis B: Environmental, 2011, 101(3–4): 246–255
41. Olcese R, Bettahar M M, Malaman B, Ghanbaja J, Tibavizco L, Petitjean D, Dufour A. Gas-phase hydrodeoxygenation of guaiacol over iron-based catalysts. Effect of gases composition, iron load and supports (silica and activated carbon). Applied Catalysis B: Environmental, 2013, 129: 528–538
42. Valle B, Castaño P, Olazar M, Bilbao J, Gayubo A G. Deactivating species in the transformation of crude bio-oil with methanol into hydrocarbons on a HZSM-5 catalyst. Journal of Catalysis, 2012, 285 (1): 304–314
43. Ibáñez M, Valle B, Bilbao J, Gayubo A G, Castaño P. Effect of operating conditions on the coke nature and HZSM-5 catalysts deactivation in the transformation of crude bio-oil into hydrocarbons. Catalysis Today, 2012, 195(1): 106–113
44. Guo J, Lou H, Zheng X. The deposition of coke from methane on a $Ni/MgAl_2O_4$ catalyst. Carbon, 2007, 45(6): 1314–1321